International Journal of Mechanical and Industrial Technology ISSN 2348-7593 (Online)
Vol. 14, Issue 1, pp: (10-28), Month: April 2026 - September 2026, Available at: www.researchpublish.com

FLAT PLATE SOLAR COLLECTOR OPTIMIZATION USING DESIGN OF EXPERIMENTS APPROACH

[1]ENG - MUATH ALNUAIMI, [2]ENG - BADER ALFADLY

DOI: https://doi.org/10.5281/zenodo.19680666

Published Date: 21-April-2026

Abstract: **This report aims to optimize the typical flat plate solar collector for the domestic solar heating system, considering improving solar collector efficiency and the useful solar energy gain enhancement. Consequently, piping costs and pumping power will be reduced compared to the conventional flat plate solar collector to get a compact and lightweight structure. They considered the flow distribution, which is crucial to enhancing the solar collector efficiency. Numerical studies were performed at two serpentine tube solar collector diameters (8 mm and 6 mm); both are identical in wall thickness, number of tubes, number of bends, the distance between tubes, and tube length. Several tube lengths are applied to each diameter to optimise, design, and evaluate the performance of both the serpentine tube collector energy gain and the economic benefits. Thermodynamic and heat transfer improvements are considered in this study applied to both models. Where the Reynolds number and the Dean number are significantly higher for the 6 mm tube, about five times, in contrast to the 8 mm tube. The serpentine tube length to diameter ratio (L/d) for the 6 mm diameter tube is 33 % higher than that for the 8 mm diameter tube, which reveals the thermodynamic and heat transfer performance enhancement of the collector tubes. Tube diameter variations have no significant influence on fin efficiency (absorber plate), but it has a considerable influence on the breadth reduction, which ranges between 91 % to 98 %. The tube collector efficiency of the 6 mm tube ranges among 78% to 94% in contrast to the 8 mm tube, which drops to 74% to 89%. Moreover, the heat removal factor F_R of the serpentine tube collectors' 6 mm and 8 mm is 98% and 91%, respectively. The fluid pressure drops in the serpentine tube collector correspond to tube diameter and length, while the pressure drop of the 8 mm tube ranges between 55 % to 80 % of the 6 mm tube for all tube lengths investigated. The annual collector heat gain of the 6 mm serpentine tube collector is 3982.5 W, which is approximately 25 % higher than that of the 8 mm serpentine tube collector. The financial analysis of the 6 mm serpentine tube collector shows a reduction of 22 % when compared to the 8 mm serpentine tube collector. The Propylenglycol 38% water mixture was applied in this study as the working fluid in the serpentine tube collector to determine the optimal operation performance of all samples stated earlier. In the particular studied case, the absorber plate width is considered to prove its influence on the collector performance. Moreover, fluid pressure drop, Reynold Number, and Dean Number in the collector tube.**

Keywords: **flat plate solar collector, domestic solar heating system.**

Notation, and units

R_C	*Radius of curvature*	*(mm)*
Ac	*Cross-suction area*	(m^2)
Cp	*Specific heat*	$(kJ/kg.℃)$
$\dot{m}$	*Mass flow rate*	(kg/s)
T_m	*Mean fluid temperature*	(℃)
$T_{f,in}$	*Fluid inlet temperature*	(℃)
Q_u	*Useful heat of the collector tube*	W/m²
$\dot{Q}_u$	*Useful heat of the collector*	W/m²
Q_P	*Absorbed solar energy by the plate surface*	W/m²
U_L	*Heat transfer coefficient*	$W/(m^2.K)$
$h_{f,i}$	*Convective heat transfer coefficient*	$W/(m^2.K)$
λ_f	*Fluid thermal conductivity*	$W/(m.K)$
Pr	*Prandtl number*	
F_R	*Collector heat removal factor*	
r	*Dimensionless collector mass flow rate*	
Re	*Reynold number*	
Nu	*Nusselt number*	
De	*Dean number*	
η	*US standards solar thermal efficiency*	
F'	*Efficiency factor*	
F	*Fin efficiency*	

1. INTRODUCTION

Fossil fuels are the leading global energy source, approximately 90% of the worldwide energy. Also, the demand for such energy sources is significantly increasing as consumption is 105 times faster than nature's production. The limitation of the fossil fuel supply leads to finding an alternative and sustainable energy source. Renewable energy is a recent field of energy that natural and non-exhaustible sources of energy can produce, for example, solar energy, which is the generator of all other renewable energies. The main advantages of renewable energy are eliminating emissions, which leads to catastrophic issues such as the global warming potential GWP and air pollution, according to the carbon dioxide (CO_2) emission. Applying the solar water heating system in a residential building is considered an attractive method for house owners to reduce the electricity cost and the environmental impact of fossil fuel emissions [1].

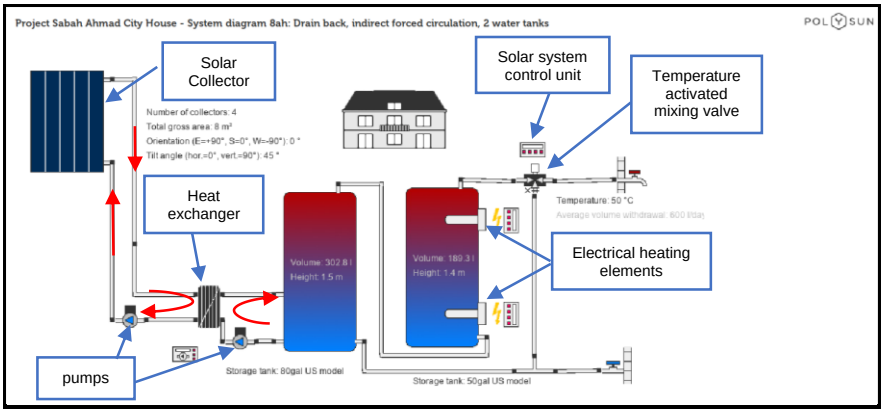

Figure 1- Solar water heating system components (Polysun Simulation Software)

The solar collector studied in this project is characterised as a non-concentrated (serpentine) continuous tubing flat plate collector. The flat plate solar collector is considered one of the solar thermal collectors; it converts the solar radiation into thermal energy and transfers it to fluid flowing through the collector tube, bonded to the absorber plate. Also, the collector is covered by glazing to allow the solar radiation to be transmitted and absorbed by the absorber plate and to avoid heat loss. Moreover, the collector edges and bottom are thermally insulated, thus improving optical and thermal efficiencies, which is crucial to improving the energy conversion in solar thermal collectors. The solar thermal system has many applications, such as domestic water and space heating. The application specifies the collector technology, which depends on the temperature range and the amount of heat energy needed. The advantages of the serpentine tube flat-plate solar collectors are simple configuration, high-pressure bearing, robust, low maintenance rate, heat efficiency even at low fluid flow, and economical. The collector's tube diameter and length contribute to the pumping power and thermodynamic performance, thus reducing the heat losses to the surroundings, keeping the mean fluid temperature T_m close to the fluid inlet temperature $T_{f,in}$ [2].

The flat plate solar collectors are non-concentrating solar thermal collecting devices commonly applied in low-temperature solar thermal systems, particularly domestic hot water applications. The flat plate solar collectors Optimization considering the improvement of thermal performance in precise techniques to achieve more absorbed solar radiation on the collector absorber plate and to transfer more thermal energy to the working fluid, in the meantime, the collector frame heat losses reduction mainly to transfer more thermal energy to the fluid flows in the collector [3]. The configuration of the flat plate solar collectors is a crucial element that affects their thermal performance. The serpentine tube solar collector performs superior to the header & riser tube collector in low-flow systems. The last beginning of turbulent flow consequently improves the heat transfer in the collector. (Oliy and Ramayya) concluded that the serpentine tube collector's internal heat transfer coefficient is advantageous over the header & riser tube collector [4]. The serpentine tube and the header riser are the main configurations of solar collectors in the domestic solar water heating system. (Deng et al., 2019) determined by CFD calculations that the collector thermal performance of the serpentine tube type is superior to that of the header riser tube type in an identical inlet temperature condition [3].

This project aims to optimise the serpentine, flat plate solar collector based on two tube diameters, 6 & 8 millimetres, with different tube bent numbers and lengths, with consistent flat plate solar collectors for domestic hot water with 2 m^2. This optimization process considers a good flow distribution, while it is crucial to enhance the solar collector efficiency. (Duffie and Beckman, 2006) stated that the fluid flow distribution through the absorber tubes highly influences flat-plate solar

collectors' thermal performance. (Chiou,1982) Investigations revealed a crucial reduction of collector efficiency beyond 20% if the flow is nonuniform. Also, it causes a significant disturbance in the collector, for instance, fluid boiling in the collector tube. Moreover, fluid flow oscillations increase the pressure drop over the collector (Fan et al., 2007). (Do Ango et al., 2013) concluded that pumping power is crucial in flat plate solar collector design and identifying the optimum circulating fluid flow to recognise the thermal behaviour constraints to obtain an economically competitive solar collector [5]. The pumping power consumption for a 1.8 m^2 panel, depending on the flow rate, ranges between 30 and 250 W (Notton et al. 2014) observed [2].

Project limitation

This study considered the serpentine tube flat plate solar collector optimization and did not consider other types of collectors or other solar heating system components. Also, the heat losses applied in this numerical calculation are limited to commercially available flat plate collectors, which are summarised in the overall heat transfer UL coefficient. Where the overall coefficient of heat transfer U_L of the 6 mm tube collector is 4.1 $W/(m^2.K)$ And for the 8 mm tube collector, U_L is 4.8 $W/(m^2.K)$. Moreover, the fluid flow in the collector tube is limited to 0.023 kg/s for the 6 mm tube collector and 0.0069 kg/s for the 8 mm tube collector; these limits avoid fluid vaporisation of low flow and hydraulic head losses. Furthermore, the project is limited to the state of Kuwait region with its specific meteorological data and other parameters. Also, the environmental analysis is not covered in this paper, while it is essential in such studies.

2. LITERATURE REVIEW & BACKGROUND

The serpentine tube is defined as a several-tube arrangement providing a large heat transfer area in a small space with high heat transfer coefficients. (Plaza Gomariz et al., 2019) stated that the serpentine tube type comes up with better efficiency than the header & riser tube type because of the advantages of fluid flow stability in the serpentine tube collector due to low fluid flow is adequate in the serpentine tube type. Hence, steady flow avoids the hot spots, which change the fluid properties and vaporize. Also, serpentine tube type is economically feasible according to low flow rate, consequently reaching the lowest initial and operation costs; smaller diameter tubes are adequate in the serpentine tube system, where low pumping power is sufficient for fluid circulation in the system [6].

(Rhoades et al., 2020) described that the serpentine tube guides the fluid flow along the curved pipe. Also, they studied the projected optimized designs and the influence of the radius of curvature R_C with the Reynolds number. Moreover, a smaller radius of curvature Rc and a more significant Reynolds number increases the centrifugal forces around the curved tube, leading to high Dean vortices. This improves the collector's internal heat transfer according to the increase of fluid homogenization [7]. (Dayan et al., 1998) reported that the serpentine tube collector performs better than the header-riser collector due to the early start of turbulent flow, which enhances the internal heat transfer coefficient, particularly in low flow. Since the increase of collector tube surface area exposed to solar radiation due to the rise of the number of turns and tube length of the collector. Also, the number of tubes in the serpentine collectors influences FR's heat removal factor.

Conversely, turbulent flow in the serpentine collectors increases the pumping power significantly, which is the downside of the serpentine tube collectors, where it's advised to be low turbulent flow as possible. (Dayan et al., 1998) reported that the serpentine collector connection in parallel is recommended to reduce the pressure drop across the system because it slightly influences the collector heat removal factor F_R [8]. Also, (Moss et al., 2017) recommended that the parallel connection of the serpentine tube absorbers increases the heat output by 1.4% in contrast with the series connection due to the low-pressure drop and high flow rate. Moreover (Moss et al.) stated that the optimum tube diameter for a flat plate collector will reduce heat losses with limited mean absorber surface temperature. Also, the pumping power is proportional to the tube length and facilitated by the parallel assembly of multiple solar collectors [2].

(Jiandong et al., 2015) studied the thermal performances of the flat-plate solar collector considering the absorber plate thickness, tube spacing, tube length, tube diameter of the collector. (Jiandong et al., 2015) realized that the optimum absorber plate thickness is about 0.9 mm, where the plate thickness is proportional to the collector efficiency. Also, found that the reduction of collector tube spacing (W) efficiently enhances the collector heat gain.

Moreover, (Jiandong et al., 2015) found that the optimum collector tube length is about 2 meters, where the enhancement for tubes length 1.2 meters and 2.8 meters is insignificant, which is about 4%. The collector tube diameter significantly enhances the collector's performance, especially under low solar radiation intensity [9].

A flow in curved tubes develops secondary flow, inducing inertial lift forces called Dean force (FD). This force disturbs the curved profile of the flow to shift from the center of the flow path towards the concave wall of the flow path. This shift

causes a pressure and velocity imbalance near the walls, which is well-known as Dean instability and leads to the form of vortices at the curvature. Dean instability flow is defined by the dimensionless number Dean number (De), representing the Dean force or force due to secondary flow in a curved tube. (Nivedita et al., 2017) reported that the strength of the secondary flow is intensely reliant on the tube A-section and radius of curvature R_C [10]. (Rosaguti et al., 2004) presents in their study of laminar flow in serpentine channels and the Dean vortices intensity and rotation influences pressure loss and heat transfer. Also, the bend direction and Reynolds number rely on the ratio of the length versus diameter (L/d) on pressure loss and heat transfer performance. (Rosaguti et al.) found the influence of the normalized friction factor increases only slightly with increasing Reynolds number, unlike the heat transfer performance; however, it increased by a factor of three over the range of Reynolds numbers in the serpentine channels. (Rosaguti et al., 2004) found the influences of the serpentine tube length to diameter ratio (L/d) on the heat transfer performance, where the increase in L/d leads to an increase in heat transfer. This increase of size against diameter in serpentine tube ratio reduces the strength of the vortices developed in each bend [11].

Also (Ghobadi) found that the heat transfer coefficient for flow with high curvature region Dean number De > 50 is capable of being enhanced according to the secondary flow initiated inside the curved tubes (serpentine). This enhancement in heat transfer because the reduction in the radius of curvature R_C and increasing the tube length ratio over the tube diameter L/d lead to increased heat transfer rate and decreases the pressure drop. Moreover, low Prandtl number fluids such as water enhance the heat transfer more than the high viscosity and high Prandtl number fluids [12]. (Mansour et al., 2019) investigated and concluded an average value of the two optimal ranges of Reynolds number and Dean number providing an excellent fluid mixing within any curved tube arrangement even in the laminar flow regime, which influences the collector's fluid flow state. Also, it leads to a much lower pressure drop and low power consumption. The optimum values of Reynolds numbers (Re) and Dean number (De) for optimal mixing are $Re_{opt} \approx 35$ at $De_{opt} \approx 10$ and $Re_{opt} \approx 650$ at $De_{opt} \approx 185$ [13].

(Moss et al., 2017) found the key factors that influence the thermal performance of the serpentine tube; these factors are summarized in the tube diameter (D), Reynold number (Re), heat removal factor (F_R), mass flow rate ($\dot{m}$) and diameter/pitch ratio (R). Moreover, (Moss) recommended the optimum diameter of the solar collectors' tubes in the range 6–16 mm reliant on pumping power and diameter/pitch ratio. Where efficiency increases with diameter/pitch ratio increase, as the (R) ratios lead to reduced mass flow rates according to tube length increases [2]. Moreover, mass flow rate increase leads to a rise in Reynolds number, hence, changes the flow in the collector tubes from laminar to turbulent flow. Consequently, it improves the heat transferred to the working fluid. Furthermore, (Helvaci et al., 2015) stated that the mass flow rate and solar radiation greatly influence the collector size and heat transfer coefficient of the fluid. The operating pressure does not affect the collector tube length [14].

(Do Ango et al., 2013) observed that the air gap thickness has a considerable impact on the solar collector's performance and efficiency. The glazing heat losses decrease significantly by the insulating effect of the air gap thickness between the collector glazing and the collector tubes absorber. This results from convection dominating the conduction in the solar collector air gap [5]. (Do Ango et al.), found that the optimal solar collector air gap 10 mm. (Moss et al., 2017) proposed an additional measure to employ vacuum to eliminate gaseous conduction using evacuated panels and reduce the heat loss coefficients to UL 1W=m2 K [2].

3. METHODOLOGY

The numerical study based on the monthly average temperature of the water entering the solar collector $T_{in,av}$ which is assumed to be equal to the soil temperature of the water supply system mainline is in the underground as surveyed and examined by (Al-Sanad et al., 1992) [15]. Also, the analysis is based on four representative samples of Kuwait's global horizontal irradiation (GHI), which is represented by the symbol (I), the range is 600 w/m^2, 700 w/m^2, 800 w/m^2, 900 w/m^2, and 1000 w/m^2[16].

Solar Collector Design Specification & Parameters

As illustrated in the table (1and 2), a numerical study of the solar collector applied for two diameter tube sizes with seven geometric configurations, the optimum thermal output performance, fluid flow in the collector tubes, and the manufacturing cost of the collector tubes according to their geometric structure.

Numerical study and optimization parameters:

The study was implemented to compare the result of various commercially available physical components of the flat plate solar collector. Initially, the study performed 6 mm and 8 mm outer diameter tubes as the base constraint of the analysis. Secondly, the solar collector frame size is limited to 2 meters × 1 meter, the thermal panel area (absorber area) is 1.8 m^2 and 1.9 m^2. Thirdly, each module consists of 13, 15, 15, 17, 20, 23, and 28 copper serpentine tube arrangement segments,

respectively. Fourthly, the tube pitch [W] (distance between tubes) is 0.072, 0.087, 0.102, 0.112, 0.122, 0.136, 0.150 meter respectively. Fifthly, the solar irradiance (perpendicular to panel) are 600, 700, 800, 900, 1000 W/m², respectively. Sixthly, the fluid studied in all models is the 38% water/glycol mixture. Seventhly, the total pipe length for each model is 10.7, 12.3, 12.3, 13.9, 16.3,18.7, and 22.7, respectively. Table (1) illustrate the studied solar collector optimization parameters.

Table 1 - Solar Collector Optimization Parameters

Solar Collectors Optimisation Parameters			
Total thermal panel area (absorber area) / m2	1.9		1.8
Tube outer diameter D,o / mm	8		6
Tube internal diameter D,I / mm	7.23		5.64
Transmission-absorbance product (τα)	0.85		0.87
Heat loss coefficient (UL) - W/(m².K)	4.8		4.1
Tube Pitch (Distance Between Tubes) / Meter	0.072	0.087	0.102
	0.112	0.122	0.136
		0.150	
Irradiance (perpendicular to panel) G - W/m²	600 700 800 900 1000		
Fluid	38% mixture Water/Glycol		
Plate material	Aluminium plate absorber of 0.4mm		

Energy analysis

Solar collector energy balance & governing equation

The energy balance of the flat-plate solar collector is divided into an external and internal energy balance of absorber as demonstrated by the governing equation of the system in equations (1) and figure (2). The external energy balance of the absorber is summarized by heat flow from the absorber surface to the ambient environment; the heat losses of the collector and the quality of the solar collector envelope are illustrated in equations (3, 4, 5, and 6) [17].

$$\frac{dQ}{dt} = \dot{Q}_s - \dot{Q}_{I,o} - \dot{Q}_{I,t} - \dot{Q}_u$$

Equation 1 - Governing Equation

The solar collectors run under steady-state conditions, $\frac{dQ}{dt} = 0$, $\dot{Q}_u = \dot{Q}_s - \dot{Q}_{I,o} - \dot{Q}_{I,t}$.

Also, the amount of useful energy absorbed by working fluid per unit time is:

$$\dot{Q}_u = \dot{m}\, C_p \left(T_{f,out} - T_{f,in}\right) = A_C\, F_R \left[(\tau\alpha)I - U_L\left(T_{f,in} - T_{amb}\right)\right]$$

Equation 2 - Useful heat removed from the collector

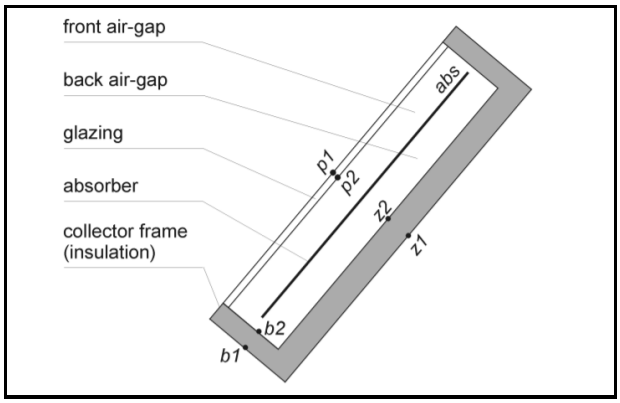

Figure 2 - Flat plate collector thermal construction [12]

The internal energy balance of the absorber is the heat flow from the absorber surface into the heat transfer fluid and the ability to transfer heat and remove it from the collector. Where the solar energy input is illustrated by equation (3).

$$\dot{Q}_s = A_C \, . I$$

Equation 3 - Solar energy input equation

The equation demonstrates the visual losses where (τα) is the practical product of transmittance–absorptance factors (4).

$$\dot{Q}_{I,o} = \dot{Q}_s - \dot{Q}_s \, (\tau\alpha)$$

Equation 4 - Visual losses equation

Then, equation (5) demonstrated the total thermal losses to the surrounding.

$$\dot{Q}_{I,t} = U . A_C \, (T_{abs} - T_{amb})$$

Equation 5 - Thermal losses equation

The efficiency can be optioned by several methods and equations based on the standards used to calculate the system energy; in this case, the US standards are used based on the fluid's specific heat as illustrated in equation (6).

$$\eta = F_R \left[(\tau\alpha) - U_L \frac{(T_{f,in} - T_{amb})}{I} \right]$$

Equation 6 - US standards solar thermal efficiency

The internal energy balance of the absorber can be exemplified by a useful heat gain equation which based on T_m fluid mean temperature as illustrated in equation (7). It also shows the effect of the absorptance property of the absorber plate and the glazing transmittance, which is presented with the Greek letters Tao τ and Alpha α, respectively [18].

$$\dot{Q}_u = A_C \, F' \left[(\tau\alpha) - U_L \left(\frac{T_m - T_a}{I} \right) \right]$$

Equation 7 - Useful heat gain equation which based on T_m

Where, T_m the mean fluid temperature is $T_m = \frac{(T_{f,out} + T_{f,in})}{2}$, and the efficiency factor F' is illustrated in equation (8) related to absorber design shown in figure (3). Moreover, the welded bond conductance C_b . Equation (9) shows the geometry and the quality of contacts between the absorber and the tube, as it influences the heat transfer as a good metal to metal contact is essential [18].

$$F' = \frac{\frac{1}{U_L}}{W \left[\frac{1}{U_L [2a + (W - 2a)F]} + \frac{1}{C_b} + \frac{1}{h_{fi} \, \pi \, D_i} \right]}$$

Equation 8 - Efficiency factor F'

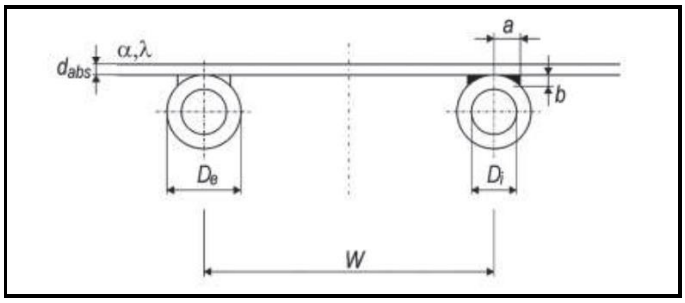

Figure 3 – Absorber & tubes design (Matuska T)

$$C_b = \frac{\lambda_b \, a}{b}$$

Equation 9 - Bond conductance C_b

Equation (10) represents the expression of the convection heat transfer inside the collector tube at laminar flow conditions, which is shown in equation (10) as the convection part of the equation [18].

$$\frac{1}{h_{fi}\,\pi\,D_i}$$

Equation 10 - Convection heat transfer inside the collector tube

As shown in figure (3), where (W) expresses the width of the absorber between two pipes, equation (11) represents the term of heat conduction through the plate to the welded bond and then to the tube within its flowed fluid.

$$\frac{1}{U[2a+(W-2a)F]}$$

Equation 11 - Conduction equation of the absorber

The convective heat transfer coefficient of flowing fluid through the collector riser tube is given by equation (12).

$$h_{f,i} = \frac{N_u\,\lambda_f}{D_i}$$

Equation 12 - Convective heat transfer coefficient

where $h_{f,i}$ is the flow convective heat transfer coefficient, D_i is the collector riser internal diameter, λ_f is the fluid thermal conductivity, N_u is the working fluid the Nusselt number [18]. Nusselt number can be obtained by equation (13), where the surface heat flux is constant and fully developed single-phase laminar flow (Re < 2300) in a circular tube, Nusselt (Nu) number is constant and independent from Reynolds (Re) and Prandtl (Pr) numbers [25].

$$Nu = \frac{h_{f,i}\,D_i}{\lambda_f} = 4.36$$

Equation 13 - Nusselt number

F is the Fin efficiency represented by equation (14) which is in Efficiency factor F' equation

$$F = \frac{tanh\left[m\left(W-D_{O/2}\right)\right]}{m\left(W-D_{O/2}\right)}\,,where\ m\ = \sqrt{\frac{U_T}{k_\delta}}$$

Equation 14 - Fin efficiency

Finding the Reynolds and Prandtl number of the fluid to obtain the Nusselt number illustrated in the equations (15 & 16), respectively, where μ is the dynamic fluid viscosity and the rest parameters are shown previously [18].

$$Re = \frac{4\,\dot{m}_{riser}}{\pi\,D_i\,\mu}$$

Equation 15 - Reynolds number

$$\mathrm{Pr} = \frac{\mu\,c_p}{\lambda_f}$$

Equation 16 - Prandtl number

Solar collector efficiency equation

The efficiency of the flat plate collector is an indication of the solar collector's performance, where it is the fraction of the useful energy gain Q_u to the solar energy gained by the solar collector, as illustrated in equation (17). Where, $\dot{m}$ is the mass flow rate, C_P is the specific heat, and the Δt is the inlet and outlet temperature difference of the solar collector fluid. In addition, the solar collector area A_C, and the solar irradiance I_T [19]. For more clarification, Δt is the difference between $T_{f,in}$ inlet fluid temperature of the solar collector, and the outlet liquid temperature $T_{f,out}$ of the solar collector, illustrated on the left side of the solar collector, useful heat removed equation (17).

$$\eta = \frac{\dot{m}\,C_p\,\Delta t}{A_C\,I_T}$$

Equation 17 -Flat plate collector's efficiency equation

Useful heat removal from the solar collector equation

The Useful heat removed from the solar collector, illustrated in equations (18), demonstrates the solar energy obtained by a specific solar collector [18]. The right side of the equation parameters is A_C the collector area, F_R the solar collector heat removal factor, τ the glazing cover transmittance, α the absorptance of the absorber plate, I_T the solar radiation incident on the collector surface, U_L the collector's overall heat loss coefficient, T_{amb} the ambient temperature, $T_{f,in}$ the fluid inlet temperature. The left side of the equation is demonstrated in the solar collector efficiency section.

$$\dot{Q} = \dot{m}\, C_p \left(T_{f,out} - T_{f,in}\right) = A_C\, F_R \left[(\tau\alpha)I - U_L\left(T_{f,in} - T_{amb}\right)\right]$$

Equation 18 - Useful heat removed from the collector

Moreover, the collector heat removal factor can be obtained using equation (19), and the efficiency factor F′ can be obtained using the dimensionless collector mass flow rate (r) which is illustrated in equation (20).

$$F_R = \frac{\dot{m}\, C_p \left(T_{f,out} - T_{f,in}\right)}{A_C \left[(\tau\alpha)I - U_L\left(T_{f,in} - T_{amb}\right)\right]}$$

Equation 19 - Collector heat removal factor

$$r = \frac{\dot{m}\, C_p}{A_C\, U_L\, F'}$$

Equation 20 - Dimensionless collector mass flow rate

Thermodynamic and Mass flow properties influence

Dean number (D_e) is a crucial factor influencing the curved tube's fluid flow and heat transfer. While it relies on the Reynolds number (R_e), the internal tube diameter (D_i), and the tube radius of the curvature (R_C) as demonstrated in equation (21) [20].

$$D_e = R_e \sqrt{\frac{D_i}{2\, R_C}}$$

Equation 21 - Dean Number

Iteration Process

The numerical model is created to simulate the serpentine tube flat plate solar collector operation. The solar collector design specification & parameters for 6 mm and 8 mm tubes are presented in tables (1, 2, and 3). Mainly, the model relies on dividing the serpentine collector tube into finite elements to calculate the fluid outlet temperature ($T_{f,out}$), plate temperature (T_{p}), the useful heat Q_u, and the heat gain ($\dot{Q}_u$) iteratively. Every single element sets the inlet value of the following element equal to the outlet value of the former element, up to the end of the last element. The overall heat transfer coefficient U_L is set to 4.1 W/(m².K) for the 6 mm tube collector and 4.8 W/(m².K) for the 8 mm tube collector to calculate each model. Initially, approximate an arbitrary value for (T_{p}) 5℃ higher than the fluid inlet temperature ($T_{f,in}$). Then, the model evaluates useful heat (Q_u) by using the overall coefficient of heat transfer U_L for the 6 mm and 8 mm serpentine tube collector in equation (22).

$$Q_u = A_C\, F_R \left[(\tau\alpha)I - U_L\left(T_{f,in} - T_a\right)\right]$$

Equation 22 - Useful Heat

Before calculating the heat transfer coefficient, the fluid flow condition should be defined by determining the Reynolds number (Re) of laminar or turbulent fluid flow in the collector tubes. After that, the Nusselt number (Nu) is calculated based on the Reynolds number (Re) for laminar fluid flow (Re < 2300). While the Nusselt number (Nu) for both collector tubes is illustrated in equation (13). Then the heat transfer coefficient is calculated by using equation (12). Initially, the plate temperature (T_p) are estimated to determine the initial fluid mean temperature ($T_{f,m}$), where the outlet temperature of the fluid is unknown, the mean fluid temperature is defined in equation (23).

$$T_{f,m} = \frac{T_p + T_{f,in}}{2}$$

Equation 23 - Fluid mean temperature

Then, the entire collector tube's useful heat is calculated by equation (24).

$$Q_u = \dot{Q}_u \, \pi \, D_i \, L_{tube}$$

Equation 24 - Useful heat of the collector tube

Where ($\dot{Q}_u$) represent the useful heat rate and ($\pi \, D_i$) is the surface perimeter. Hence, the useful heat rate ($\dot{Q}_u$) achieved by dividing useful heat (Q_u) by the collector surface area ($\pi \, D_i \, L_{tube}$) as illustrated in equation (25).

$$\dot{Q}_u = \frac{Q_u}{\pi \, D_i \, L_{tube}}$$

Equation 25 - Useful heat of the collector

Later, the heat gain for each finite element is calculated by multiplying the useful heat rate by the surface perimeter, then by the length of each finite element. Which was defined previously in equation (24). So, the heat gain of each finite element is calculated by equation (26)

$$Q_{\text{gain}} = \dot{Q}_u \, \pi \, D_i \int_0^L dx$$

Equation 26 - Heat gain for each finite element

Instantly, the heat gain is determined for the first element of fluid outlet temperature ($T_{f,out}$) computed using equation (27).

$$T_{f,out} = T_{f,in} + \frac{Q_{\text{gain}}}{\dot{m} \, C_p}$$

Equation 27 - Fluid outlet temperature

Then again, a new mean temperature ($T_{f,m}$) calculated by the equation (28) by using the first element of fluid outlet temperature ($T_{f,out}$).

$$T_{f,m} = \frac{T_{f,in} + T_{f,out}}{2}$$

Equation 28 - New mean temperature

Hence, the absorbed solar energy on the surface of the plate Q_P or in other words, the new useful heat of the collector tube Q_u are calculated with the new plate temperature (T_p) using the last calculated (new) mean temperature ($T_{f,m}$) by applying the equations (29 & 30) respectively.

$$T_p = T_{f,in} + \frac{Q_u / A_C}{F_R \, U_L} \, (1 - F_R)$$

Equation 29 - New plate temperature

$$Q_P = A_C \, [(\tau\alpha) I - U_L (T_P - T_a)]$$

Equation 30 - Absorbed solar energy by the plate surface

Finally, the iteration process was repeated using the previous method by re-evaluation of the Q_u and Q_{gain} applying the new plate temperature (T_p) and new fluid outlet temperature ($T_{f,out}$) resulted for each iteration loop. This iteration process is repeated until the difference between the new (T_p) and the new ($T_{f,out}$) for both previous iteration temperatures reach the lower convergence criteria of 0.01 ℃ [14].

Design of Experiments Optimization Procedure

The optimization Procedure of the project is separated into seven steps to achieve the project aims and the general objective; the steps are illustrated as follows:

1. Problem Recognition

2. Response variable selection

3. Factors, levels, and ranges selection

4. Experimental design selection

5. Experiment execution

6. Data statistical analysis

7. Conclusions and recommendations

The basic principles of design of experiments (DOE) are randomisation, replication, blocking, and factorial. The statistical randomisation methods are the backbone of the experimental design by performing a random individual run for experimental allocation factors [21]. The first-order model fitting the 8-parameter in n^k, $or\ 2^3, where\ \kappa = 3$ factors illustrated in equation (31):

$$y\hat{} = \beta_0 + \beta_1 x_1 + \beta_2 x_2 + \beta_3 x_3 + \beta_{12} x_1 x_2 + \beta_{13} x_1 x_3 + \beta_{23} x_2 x_3 + \beta_{123} x_1 x_2 x_3$$

Equation 31- Factorial Designs Response

where $y\hat{}$ is the response, the x's are the design factors, the β's are unknown parameters estimated from the data in the experiment, and the random error term is ∈. Also, the cross-product term $\chi_1 \chi_2$, $\chi_2 \chi_3$, and $\chi_1 \chi_3$ represents the interaction between the design factors. Moreover, the Sum of Squares (SS) for solar collector tube diameter is

$$SS_{\text{Tube Diameter}} = \frac{1}{bcn}\sum_{i=1}^{a} y_{i\ldots}^2 - \frac{y_{\ldots\ldots}^2}{abcn}$$

, the collector tube price in $

$$SS_{\text{Price in \$}} = \frac{1}{acn}\sum_{j=1}^{b} y_{.j..}^2 - \frac{y_{\ldots\ldots}^2}{abcn}$$

, and the useful heat gain of the collector tube

$$SS_{\text{Useful Heat Gain}} = \frac{1}{abn}\sum_{k=1}^{c} y_{..k.}^2 - \frac{y_{\ldots\ldots}^2}{abcn}$$

4. RESULTS AND DISCUSSION

Flat Plate Solar Collector Design

This work aims to optimize a serpentine solar collector pipe within the commercial copper tubes dimensions for a specific diameter, thickness, riser number, bent number, and tube length. This work relates to a typical flat plate solar collector's configuration for domestic hot water with 2 m^2. The outer diameter of the optimized serpentine solar collector pipe is 8 mm and 6 mm, with a wall thickness of 0.71 mm for both tubes. Tables (4 and 5) illustrate the experimental model's physical and thermodynamic parameters analysed to optimise the serpentine solar collector tube. The 6 mm tube collector presents a much better flow distribution, where the Reynolds number is more than five times higher than that for the 8 mm tube collector, where it is for 6 mm is R_e=1582, and 8 mm is R_e=278. In addition, Dean number behaves similarly to the Reynolds number manner, where the 6 mm tube collector is approximately five times greater than the 8 mm tube collector, where the D_e for the 6 mm tube collector ranges between 970 and 1420, and the D_e for the 8 mm tube collector ranges between 193 and 283. This change in Dean number D_e depends on the tube bent radius of curvature R_C and tube diameter differences. Moreover, the 6 mm tube collector has the advantage of a high flow rate and high flow speed compared to the 8 mm tube collector, approximately four times and seven times, respectively, as illustrated in Tables 2 and 3.

Table 2 - Thermodynamics Parameters of 6 mm Serpentine Tube TYPE (B6)

Thermodynamics Parameters of the 6 mm Serpentine Tube TYPE (B6)

Radius of Curvature Rc (mm)	Pipes Number	Bent Number	Pipe length (Meter)	Curvature Ratio	Outer Dimeter (mm)	Internal Dimeter (mm)	A Cross-sectional area (Meter)	Flow Rate m^3/s	Dean Number D_e	Reynolds Number R_e	flow speed (m/s) u
7.5	13.0	12.0	10.7	0.8					970		
7.0	15.0	14.0	12.3	0.8					1019		
6.5	15.0	14.0	12.3	0.9					1042		
6.0	17.0	16.0	13.9	0.9	6	5.3	2.4971E-05	3.0833E-05	1085	1582	1.235
5.5	20.0	19.0	16.3	1.1					1177		
4.5	23.0	22.0	18.7	1.3					1281		
3.5	28.0	27.0	22.7	1.6					1420		

Table 3 - Thermodynamics Parameters of 8 mm Serpentine Tube TYPE (B8)

Thermodynamics Parameters of the 8 mm Serpentine Tube TYPE (B8)

Radius of Curvature Rc (mm)	Pipes Number	Bent Number	Pipe length (Meter)	Curvature Ratio	Outer Dimeter (mm)	Internal Dimeter (mm)	A Cross-sectional area (Meter)	Flow Rate m^3/s	Dean Number D_e	Reynolds Number R_e	flow speed (m/s) u
7.5	13.0	12.0	10.7	1.0					193		
7.0	15.0	14.0	12.3	1.1					203		
6.5	15.0	14.0	12.3	1.1					207		
6.0	17.0	16.0	13.9	1.2	8	7.3	4.1034E-05	6.9444E-06	216	278	0.169
5.5	20.0	19.0	16.3	1.4					234		
4.5	23.0	22.0	18.7	1.7					255		
3.5	28.0	27.0	22.7	2.1					283		

Figure 4 demonstrates the tube design and configuration of both tube sizes examined in this project to show the limitation of the tube room in the standard collector frame. SOLIDWORKS 3D CAD 2019 package used to design the physical dimensions of the collector and its components.

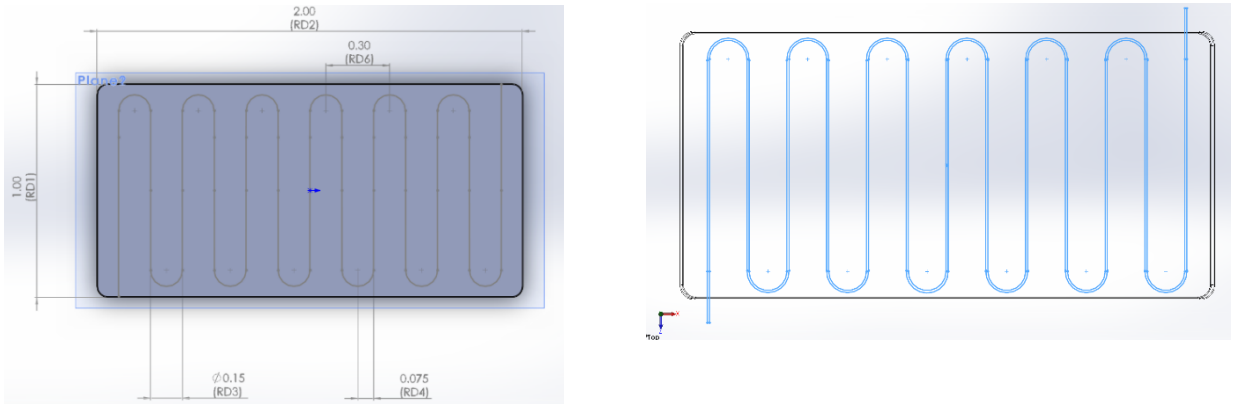

Rc 7.5, 10.7 m tube length

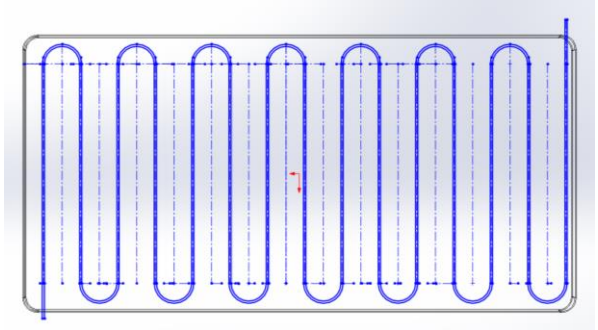

Rc 6.5 & Rc 7, 12.3 m tube length

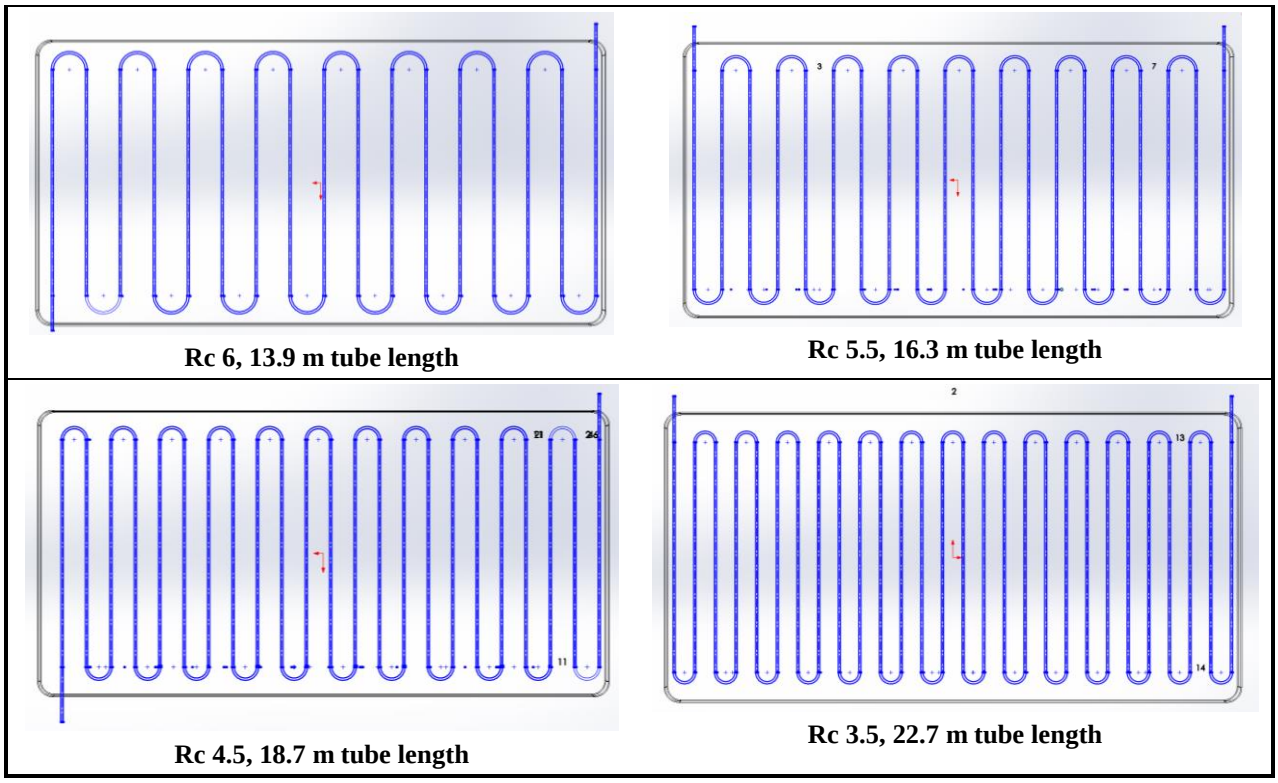

Figure 4 - Tube design & configuration

5. ANALYSIS

Length to Diameter Ratio Analysis

The serpentine tube length to diameter ratio (L/d) influences the heat transfer performance and decreases the pressure drop. The intended length in this ratio is the tube length between two curved tubes (bend). Tables (6 and 7) represent the influences of the (L/d) ratio, which investigated for 6 mm and 8 mm serpentine tubes. The (L/d) ratio reduced with the increase of total pipe length, where the (L/d) ratio for the 6 mm diameter tube declined from 25, 23.33, 21.67, 20, 18.33,15, and 11.67 for the observed tube length 150 mm, 140 mm, 130 mm, 120 mm, 110 mm, 90 mm, and 70 mm respectively as illustrated in a table (4).

Table 4 - Tube length ratio over the tube diameter (L/d) for 6 mm & 8 mm diameter

Radius of Curvature Rc	Pipes Number	Bent Number	Pipe length	Pipe length	L	Tube TYPE (B8)			Tube TYPE (B6)		
						d	(L/d)	(Rc/d)	d	(L/d)	(Rc/d)
(mm)			(mm)	(Meter)	(mm)	(mm)	Ratio	Ratio	(mm)	Ratio	Ratio
7.5	13	12	10683	10.68	150		18.8	0.94		25.0	1.25
7.0	15	14	12308	12.31	140		17.5	0.88		23.3	1.17
6.5	15	14	12286	12.29	130		16.3	0.81		21.7	1.08
6.0	17	16	13901	13.90	120	8	15.0	0.75	6	20.0	1.00
5.5	20	19	16328	16.33	110		13.8	0.69		18.3	0.92
4.5	23	22	18711	18.71	90		11.3	0.56		15.0	0.75
3.5	28	27	22697	22.70	70		8.8	0.44		11.7	0.58

Likewise, the (L/d) ratio for the 8 mm diameter tube declined from 18.75, 17.5, 16.25, 15, 13.75,11.25, and 8.75 for the examined tube length 150 mm, 140 mm, 130 mm, 120 mm, 110 mm, 90 mm, and 70 mm respectively as illustrated in a table (6).

Fins Efficiency Analysis

The fin efficiency in this study represents the absorber plate efficiency bonded to each tube of the studied solar collector. Figure (5) shows the fin efficiency variation for the 6 mm and the 8 mm diameter tubes of the absorber plate widths. As illustrated, there is no significant influence on the tube diameter difference. But it shows a considerable impact on the absorber plate width. The fin efficiency is inverse to absorber plate width; fin efficiency decreases with the absorber plate width increase.

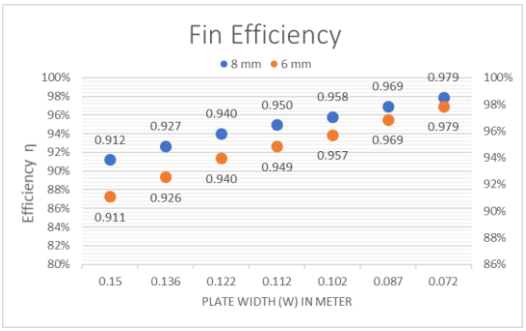

Figure 5 -Fin Efficiency for collectors

Annual Collectors Efficiency Analysis

The annual collector efficiency is crucial in showing the collector's performance. Figure (6) illustrates the efficiency of both tube diameters studied in this project and the expected solar irradiance range of the region. This analysis shows the merit of the 6 mm tube collector efficiency, which ranges between 78% to 94% over the 8 mm tube collector efficiency, which falls between 74% to 89%.

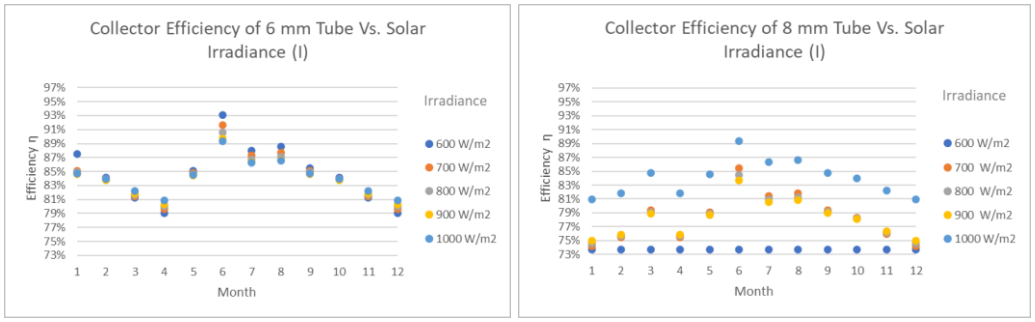

Figure 6 - Annual Collector Efficiency for 6 mm & 8 mm Dimeter tube Vs. Solar Irradiance

Collectors Heat Removal Factor Analysis

The collector heat removal factor (F_R) represents the ratio of the actual heat transfer to the maximum possible heat transfer through the collector plate. This study distinguished the 6mm tube collector's heat removal factor over the 8 mm tube collector. The collector heat removal factor of the 6mm tube collector is 98% and 91% for the 8 mm tube collector. Moreover, the plate width (W) does not affect the collector heat removal factor. The heat removal factor is identical for each plat width of each analysed tube diameter, as shown in figure (7).

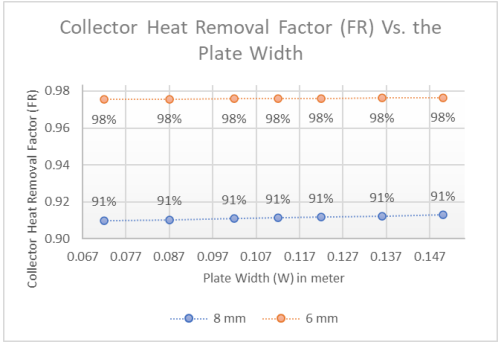

Figure 6 - The collector heat removal factor of the 6mm & 8 mm tube collector

Fluid Pressure Drop Analysis

The serpentine tube collector diameter significantly influences the fluid pressure drop in the tube collector. Since the tube diameter decreases, the pressure drop increases substantially; the serpentine tube length has proportionated effects on the pressure drop. The increase in the tube length increases the pressure drop in the fluid flown in the tube, as demonstrated in Figure 8. This analysis found that the pressure drop of the 6 mm tube is much higher than that of the 8 mm tube. Where the pressure drop of the 6 mm tube is 17.6 kPa, 20.3 kPa, 23 kPa,26.9 kPa,30.9 kPa,37.5 kPa for the tube length, 10.7 m, 12.3 m, 13.9 m, 16.3 m, 18.7 m, and 22.7 m, respectively. In contrast, the 8 mm tube, the pressure drop does not exceed the 7 kPa for all tube lengths investigated.

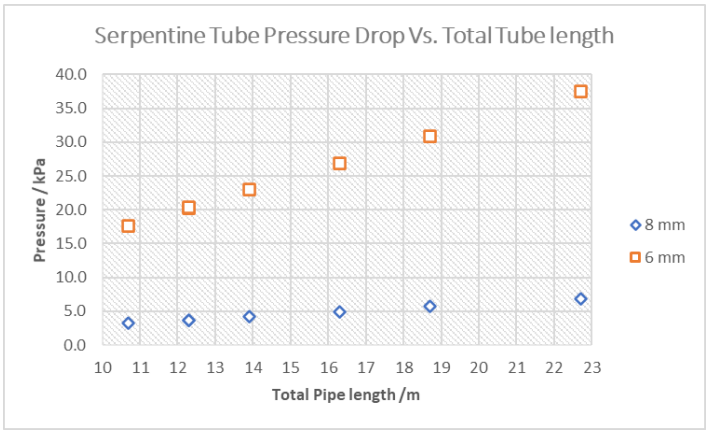

Figure 7 - Serpentine Tube Pressure Drop Vs. Total Tube length

Dean number Analysis

Dean number improves the fluid mixing within the serpentine tube arrangement even in the laminar flow regime; this improvement increases the heat transfer rate and decreases the pressure drop. This analysis illustrates the Dean number influences on each tube diameter studied in this paper, while the Dean number of the 6 mm tube is significant compared to the 8 mm tube. The Dean number of the 6 mm serpentine tube collector and its relation to the radius of curvature is 970, 1018, 1042, 1084, 1176, 1281, 1420 In contrast to 7.5 mm, 6.8 mm, 6.5mm, 6 mm, 5.1 mm, 4.3 mm, and 3.5 mm respectively. On the other hand, the Dean number of the 8 mm serpentine tube collector is 193, 202, 207, 215, 234, 254, and 282, in contrast to the same radius of curvature the previous 6 mm tube. This analysis is demonstrated in figure (9).

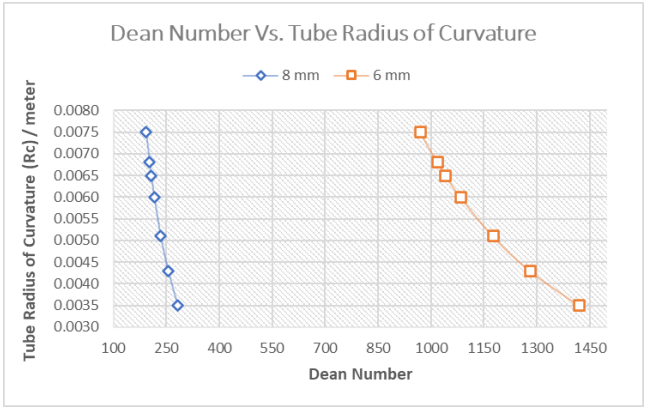

Figure 8 - Dean Number Vs. Tube Radius of Curvature

Collectors Heat Gain Analysis

The collector heat gain exposes the most critical factors affecting the performance of the serpentine tube collector. The 6 mm serpentine tube collector, ranging between 3797.6 Watt in January to 3982.5 Watt in June. Also, the collector heat gain difference between tubes length is negligible. On the contrary, the annual collector heat gain of the 8 mm serpentine tube collector declines, ranging from 2836 Watt to 3013 Watt. Moreover, the difference in tube length is insignificant to the collector heat gains, which is approximately 4%, as illustrated in figure (10).

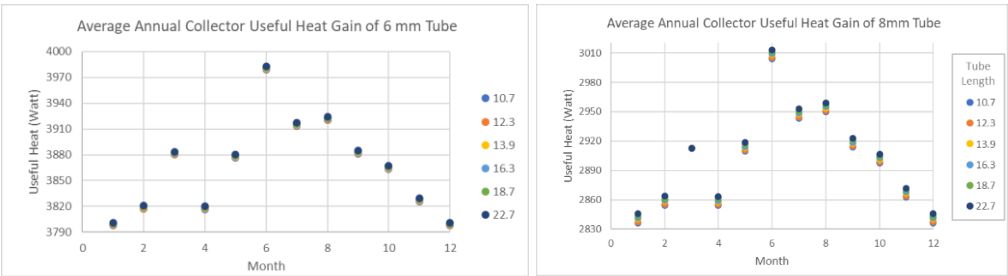

Figure 9 - Average Annual Collector Useful Heat Gain of 6 mm & 8 mm Serpentine Tube

Financial Analysis

The financial analysis of the 6 mm and 8 mm copper tubes used in this study illustrates the key parameters that influence the cost of the solar collector tube. Tables (8) describe the variation of the tube radius of curvature (Rc), Distance between pipes (W), total pipe length & weight, and the total price for each pipe length for each collector standard frame. The copper tube type (B) for 6 mm diameter size total cost for the entire solar collector used in the study ranges from 7.6, 8.8, 9.9, 11.7, 13.4, and 16.2 US. $ for tube length 10.7, 12.3, 13.9, 16.3, 18.7, and 22.7 meters, respectively.

Table 5 - Financial analysis of a 6 mm & 8 mm copper tube

TYPE B – Copper Tubes B8 & B6

SCHEDULE DESIGNATIONS	NOMINAL PIPE SIZE		OD	ID	WALL THICKNESS	WEIGHT
	INCH	MM	MM	MM	MM	KG/Meter
Copper Tubes B8	1/4	8	7.94	7.23	0.71	0.143
Copper Tubes B6	1/8	6	6.35	5.64	0.71	0.112

Radius of Curvature R_C	No. of Pipes	No. of Bends	Distance between pipes	Total Pipe length	Total Pipe Weight	Price / Meter	Total Price for Pipe length	Price / Meter	Total Price for Pipe length
						Copper Tubes			
						B8		**B6**	
mm			Meter		Kg/Meter	US.$	US.$	US.$	US.$
3.5	28.0	27.0	0.072	22.7	3.2	0.9	20.8	0.7	16.2
4.3	23.0	22.0	0.087	18.7	2.7	0.9	17.2	0.7	13.4
5.1	20.0	19.0	0.102	16.3	2.3	0.9	15.0	0.7	11.7
6.0	17.0	16.0	0.112	13.9	2.0	0.9	12.8	0.7	9.9
6.5	15.0	14.0	0.122	12.3	1.8	0.9	11.3	0.7	8.8
6.8	15.0	14.0	0.136	12.3	1.8	0.9	11.3	0.7	8.8
7.5	13.0	12.0	0.150	10.7	1.5	0.9	9.8	0.7	7.6

Similarly, the copper tube type (B) for an 8 mm diameter size total cost for the entire solar collector used in the study ranges from 9.8, 11.3, 12.8, 15, 17.2, and 20.8 US. $ for tube length 10.7, 12.3, 13.9, 16.3, 18.7, and 22.7 meters, respectively. This shows the diameter size influence on the total solar collector tube cost. As illustrated in Table 5, the collector tube sizes are identical in wall thickness, tubes and curves quantity, the distance between tubes (absorber width – W), and the total tube length for the two sets of tube diameters in the analysed collector.

DOE Optimization Analysis

The Design of Experiments (DOE) optimisation process was applied in this study to evaluate the optimum serpentine tube collector for the project conditions. This project uses a two-level full factorial design, where the model fits the 8-parameter (test conditions) in n^k, $or\ 2^3, where\ \kappa = 3$ factors (independent variables) at two levels of each variable. Where y is the response, the $x's$ are the design factors; the $\beta's$ are unknown parameters that will be estimated from the data in the experiment, and it is a random error term that accounts for the experimental error in the system that is being studied. While x_1 represent the tube diameter mm (A) design factors, x_2 represent the tube price US. $ (B) design factors, and x_3 represent the collector useful heat W/m^2 (C) design factors. Moreover, the cross-product term $x_1x_2x_3$ represents the three-factor interaction between the design factors. Furthermore, $\beta_1, \beta_2, and\ \beta_3$ represent the effective coefficient of each factor, respectively. The factorial designs response calculation applied in this project is illustrated in equation (32).

$$y\hat{} = \beta_0 + \beta_1x_1 + \beta_2x_2 + \beta_3x_3 + \beta_{12}x_1x_2 + \beta_{13}x_1x_3 + \beta_{23}x_2x_3 + \beta_{123}x_1x_2x_3$$

Equation 32 - Factorial Designs Response

The logical optimization procedure for the factorial designs of experiment (DOE) which applied to this project are illustrated in logic chart in figure (11). This chart explains the optimization process for each factor and levels. Where, each factor has 2 levels (high level) and (low level) which expressed by (1) and (-1) respectively as shown in table (6).

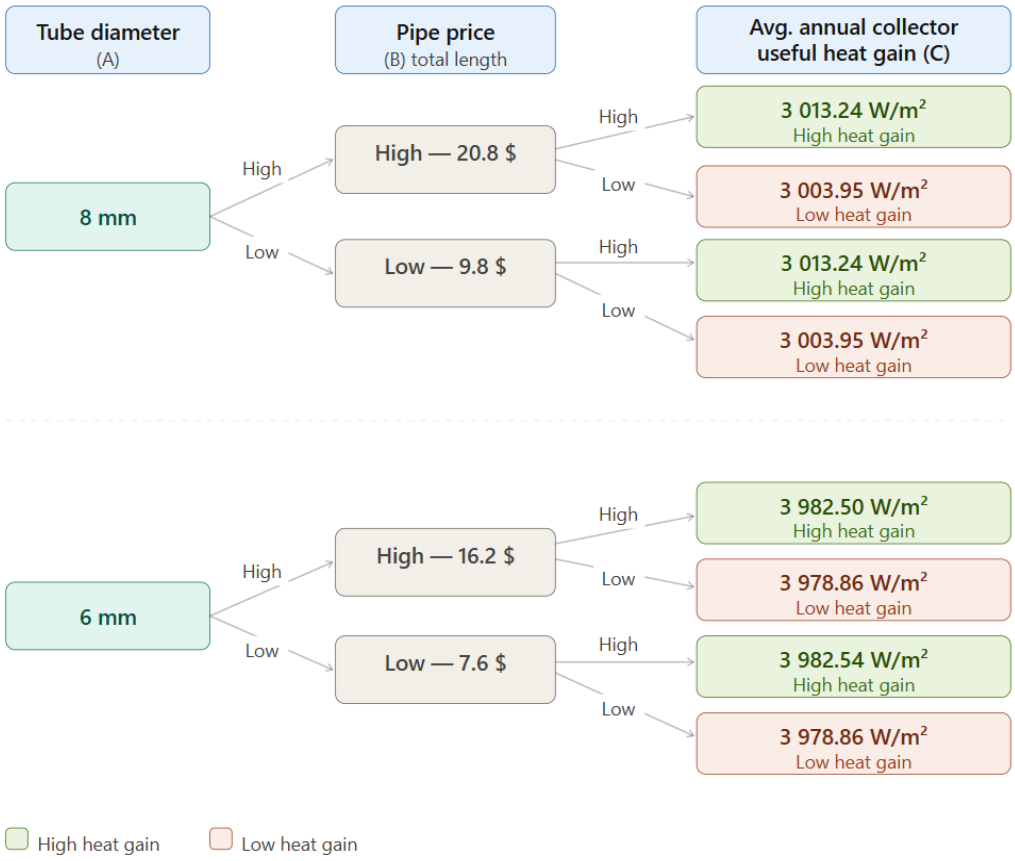

Figure 10 - Design of experiment (DOE) logical optimization procedure

Table (10) shows the factorial designs of experiment (DOE) detailed application, where each factor is expressed by the letters (A) for tube diameter, (B) for total tube price, and (C) for collector useful heat. And then, each factor has interactions with each other as presented in table (10), where the first interaction is (A.B), then (B.C), and finally (A.B.C). The (DOE) logical optimization procedure was applied to find the measurement of the model. Then the model response $y^{\wedge}$ calculated using equation (32) for all factors and levels of the model.

Table 6 - Design of Experiment Optimization Result

	Factors			Interaction			Measurement	Response
Combination	Tube Dimeter mm (A)	Total Price for Tube length $ (B)	Collector Useful Heat W/m^2 (C)	AB	BC	ABC	Runs	y^
(1)	-1	-1	-1	1	1	-1	182259.706	195888.14
a	1	-1	-1	-1	1	1	235497.4696	253547.00
b	-1	1	-1	-1	-1	1	387237.1274	376021.44
ab	1	1	-1	1	-1	-1	500348.4623	433469.58
c	-1	-1	1	1	-1	1	182427.9366	173324.30
ac	1	-1	1	-1	-1	-1	236225.9263	276886.60
bc	-1	1	1	-1	1	-1	387594.5577	353584.16
abc	1	1	1	1	1	1	501896.174	457357.18
(1)	-1	-1	-1	1	1	-1	209864.2493	195888.14
a	1	-1	-1	-1	1	1	271248.8154	253547.00
b	-1	1	-1	-1	-1	1	319039.2774	376021.44
ab	1	1	-1	1	-1	-1	412357.1612	433469.58
c	-1	-1	1	1	-1	1	209987.1303	173324.30
ac	1	-1	1	-1	-1	-1	271780.7952	276886.60
bc	-1	1	1	-1	1	-1	319226.0833	353584.16
abc	1	1	1	1	1	1	413165.8861	457357.18

Figure (12) shows that the response & probability of the model is in a straight line, which indicates that the response is normal. Then by evaluating the significance effect using the data analysis regression, the tube diameter factor is the significant value. The total tube price is the second considerable value; then, useful collector heat is the least important, as illustrated in the table (11).

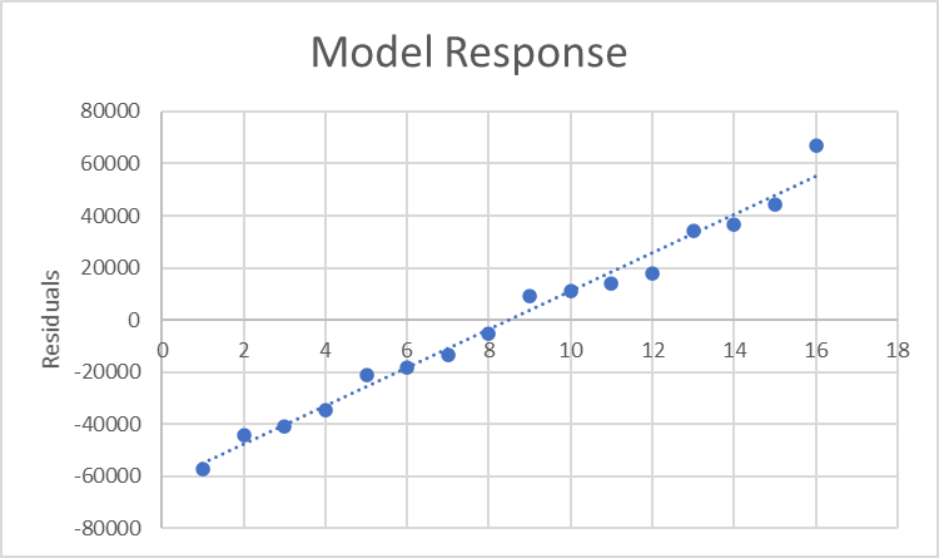

Figure 11 - Factorial Designs Response & Probability

Table 7 - Data Analysis Regression

SUMMARY OUTPUT

Regression Statistics	
Multiple R	0.9570
R Square	0.9159
Adjusted R Square	0.8599
Standard Error	40142.4703
Observations	16

ANOVA

	df	*SS*	*MS*	*F*	*Significance F*
Regression	6	1.58E+11	26333902474	16.3421	0.0002246
Residual	9	1.45E+10	1611417921		
Total	15	1.73E+11			

	Coefficients	*Standard Error*	*t Stat*	*P-value*	*Lower 95%*	*Upper 95%*	*Lower 95.0%*	*Upper 95.0%*
Intercept	315009.80	10035.62	31.3892	1.66E-10	292307.65	337711.94	292307.65	337711.94
Tube Dimeter mm (A)	40305.29	10035.62	4.0162	3.04E-03	17603.14	63007.43	17603.14	63007.43
Total Price for Tube length $ (B)	90098.29	10035.62	8.9779	8.71E-06	67396.15	112800.44	67396.15	112800.44
Collector Useful Heat W/m^2 (C)	278.26	10035.62	0.0277	9.78E-01	-22423.88	22980.41	-22423.88	22980.41
AB	11528.54	10035.62	1.1488	2.80E-01	-11173.60	34230.69	-11173.60	34230.69
BC	84.32	10035.62	0.0084	9.93E-01	-22617.82	22786.46	-22617.82	22786.46
ABC	52.68	10035.62	0.0052	9.96E-01	-22649.46	22754.82	-22649.46	22754.82

6. CONCLUSIONS

This study has identified and evaluated the performance of both the referred serpentine tube collector energy gain and the economic benefits. According to the improved flow distribution and fluid mixing even in the laminar flow regime, thermodynamics and heat transfer improvements of the 6 mm tube contrast to the 8 mm serpentine tube collector. The Reynolds number and Dean number are more than five times higher than those of the 8 mm tube collector, where the Reynolds number Re for the 6 mm is 1582, and the Dean number De for the 6 mm tube collector ranges from 970 to 1420. Also, the 8 mm Reynolds number Re is 278, and the Dean number De for the 8 mm tube collector ranges from 193 to 283. Moreover, the 6 mm tube collector has the advantage of a high flow rate and high flow speed compared to the 8 mm tube collector.

The serpentine tube length to diameter ratio (L/d) enhances the heat transfer performance and decreases the pressure drop. This ratio declined for the 6 mm diameter tube from 25 to 11.67, and the 8 mm diameter tube declined from 18.75 to 8.75 for the examined tube length range between 150 mm and 70 mm. Fin efficiency is inversely affected by the absorber plate

width, and there is no significant difference between the two collector tubes. This analysis reveals the merit of the 6mm tube collector efficiency, which ranges from 78% to 94%, in contrast to the 8 mm tube collector efficiency, which falls between 74% to 89%. The heat removal factor F_R of the analysed tubes diameter 6 mm and 8 mm, of the serpentine tube collectors is 98% and 91% tube, respectively.

On the other hand, the absorber plate width (W) does not affect the collector heat removal factor. Fluid pressure drops significantly in the serpentine tube collector as the diameter decreases. Additionally, once the serpentine tube length increases, the pressure drop in the flown fluid increases. Furthermore, this indicates that the pressure drop of the 6 mm tube is much higher than that of the 8 mm tube. Therefore, the pressure drops of the 6 mm tube range between 17.6 kPa, and 37.5 kPa. Contrastingly, the pressure drop in the 8 mm tube does not exceed the 7 kPa for all tube lengths investigated. However, the pressure drop of both tube within the acceptable range. The annual collector heat gain of the 6 mm serpentine tube collector ranges between 3797.6 W/m² and 3982.5 W/m². On the contrary, the yearly collector heat gain of the 8 mm serpentine tube collector declines to the range between 2836 W/m² and 3013 W/m². Moreover, the variation of tube length analyzed of both tube collector diameters has the least effect on annual collector heat gain of approximately 4%. The financial analysis of the studied serpentine tube collector length, ranging from 10.7 to 22.7 meters, for both studied tube diameters, shows the cost of the tube ranging between 7.6 and 16.2 US. $ for the 6 mm tube. While the 8 mm tube ranges from 9.8 to 20.8 US. $. It is found that the 6 mm serpentine tube collector exhibits higher collector efficiency than the 8 mm serpentine tube collector under the given conditions.

The design of experiments DOE optimization process applied in this study finds that the tube diameter is the significant factor over other factors used in this optimization process of the serpentine tube collector. This concludes that the numerical study can be combined with the experiments' DOE results' design to obtain the optimal product. The full factorial DOE with replicates shows a clear main effect favouring the 6 mm tube diameter (A), which clearly outperforms the 8 mm diameter, delivering 3980 W/m² collector useful heat (C) versus only 3010 W/m² for 8 mm, a significant improvement (32% higher). Within the 6 mm options, the low price of pipe length cost (B) (7.6 $) achieves essentially the same high heat output as the High price level (16.2 $), with values of 3982.54 W/m² (High) and 3978.86 W/m² (Low) being nearly identical. This configuration delivers the maximum performance according to the statistically validated model and the lowest cost. Also, as illustrated in the logical flow chart, where the a high-level logical flow is provided, while the DOE table provides the statistically analysed result.

REFERENCES

[1] Dharuman C, Arakeri JH, Srinivasan K. Performance evaluation of an integrated solar water heater as an option for building energy conservation. Energy and Buildings. 2006 Mar 1;38(3):214-9.

[2] Moss RW, Shire GS, Henshall P, Eames PC, Arya F, Hyde T. Optimal passage size for solar collector microchannel and tube-on-plate absorbers. Solar Energy. 2017 Sep 1;153:718-31.

[3] Deng J, O'Donovan TS, Tian Z, King J, Speake S. Thermal performance predictions and tests of a novel type of flat plate solar thermal collectors by integrating with a freeze tolerance solution. Energy Conversion and Management. 2019 Oct 15;198:111784.

[4] Oliy GB, Ramayya AV. Experimental Testing of a Serpentine Flat Plate Solar Water Heater. International Journal of Energy and Power Engineering. 2017 Aug 18;6(4):61.

[5] Do Ango AM, Médale M, Abid C. Optimization of the design of a polymer flat plate solar collector. Solar Energy. 2013 Jan 1;87:64-75.

[6] Plaza Gomáriz F, Cejudo-Lopez JM. Experimental comparison of serpentine and parallel-tubes flat plate collectors for different flow rates.

[7] Rhoades T, Kothapalli CR, Fodor PS. Mixing Optimization in Grooved Serpentine Microchannels. Micromachines. 2020 Jan;11(1):61.

[8] Dayan M, Klein S, Beckman W. Analysis of serpentine collectors in low flow systems. Solar Energy Laboratory University of Wisconsin-Madison. 1998;1500.

[9] Jiandong Z, Hanzhong T, Susu C. Numerical simulation for structural parameters of flat-plate solar collector. Solar Energy. 2015 Jul 1;117:192-202.

[10] Nivedita N, Ligrani P, Papautsky I. Dean flow dynamics in low-aspect ratio spiral microchannels. Scientific Reports. 2017 Mar 10;7(1):1-0.

[11] Rosaguti NR, Fletcher DF, Haynes BS. Laminar flow in a periodic serpentine channel. InProc. 15th Australasian Fluid Mechanics Conference 2004 Dec 13.

[12] Ghobadi M. *Experimental measurement and modelling of heat transfer in spiral and curved channels* (Doctoral dissertation, Memorial University of Newfoundland).

[13] Mansour M, Thévenin D, Nigam KD, Zähringer K. Generally-valid optimal Reynolds and Dean numbers for efficient liquid-liquid mixing in helical pipes. Chemical Engineering Science. 2019 Jun 29;201:382-5.

[14] Helvaci HU, Khan ZA. Mathematical modelling and simulation of multiphase flow in a flat plate solar energy collector. Energy Conversion and Management. 2015 Dec 1;106:139-50.

[15] Al-Sanad HA, Ismael NF. Thermal properties of desert sands in Kuwait. JOURNAL-UNIVERSITY OF KUWAIT SCIENCE. 1992 Jan 1;19:207-.

[16] Mpholo M, Steuerwald D, Kukeera T. Africa-EU Renewable Energy Research and Innovation Symposium 2018 (RERIS 2018): 23–26 January 2018, National University of Lesotho On occasion of NULISTICE 2018. Springer Nature; 2018.

[17] Matuska T, Metzger J, Benda V. Design tool KOLEKTOR 2.2 for virtual prototyping of solar flat-plate collectors. Proceeding of Eurosun 2008. 2008 Oct 7.

[18] Rangababu JA, Kumar K, Rao S. Numerical Analysis and Validation of Heat Transfer Mechanism of Flat Plate Collectors. Procedia Engineering. 2015 Jan 1;127:63-70.

[19] Duffie JA, Beckman WA. Solar engineering of thermal processes. New York: Wiley; 1991.

[20] Li Y, Wang X, Zhou B, Yuan S, Tan SK. Dean instability and secondary flow structure in curved rectangular ducts. International Journal of Heat and Fluid Flow. 2017 Dec 1;68:189-202.

[21] Daily JW. Design and analysis of experiments: Douglas C. Montgomery, John Wiley & Sons, New York, 1984, 538 pages, $44.50.

[22] Farahat S, Sarhaddi F, Ajam H. Exergetic optimization of flat plate solar collectors. Renewable energy. 2009 Apr 1;34(4):1169-74.

[23] Aste N, Del Pero C, Leonforte F. Thermal-electrical optimization of the configuration a liquid PVT collector. Energy Procedia. 2012 Jan 1;30:1-7.

[24] Subramanian RS. Heat transfer to or from a fluid flowing through a tube. Convective Heat Transfer I-Flow Through Conduits, Clarkson University, http://web2. c larks on. edu/proje ct s/subramanian/ch302/notes/Convective* 20Heat* 2OTransfer. 2008;201.

[25] CENGEL, Y.; HEAT, Transfer Mass. A practical approach. New York, NY, USA: McGraw-Hill, 2003.

[26] SOLIDWORKS 3D CAD 2019 package

[27] Microsoft Excel spreadsheet software program